Mechanically tunable dry adhesive from wrinkled elastomers†

Pei-Chun Lin,[ab] Shilpi Vajpayee,[c] Anand Jagota,*[c] Chung-Yuen Hui[d] and Shu Yang*[a]

Received 18th February 2008, Accepted 10th May 2008
First published as an Advance Article on the web 18th June 2008
DOI: 10.1039/b802848f

We report a new dry adhesive structure using a rippled poly(dimethylsiloxane) (PDMS) elastomer bilayer film, whose surface roughness and adhesion can be reversibly regulated by applying mechanical strain. It has a set of advantages not offered by other techniques for regulation of adhesion, including real-time tunability, no requirement of specific surface chemistry, operability under ambient conditions, and relative ease of control. To understand the mechanism for adhesion regulation quantitatively, we have modeled the mechanics of adhesion in the limits of small- and large-amplitude ripples, and show good agreement with indentation experiments. We demonstrate the real-time tunability of the new adhesive structure by repeatedly picking and releasing a glass ball simply by modulating the mechanical stretch of the rippled PDMS film.

Introduction

The ability to reversibly tune the adhesion of a material to another surface in a controlled fashion is highly desirable for many applications, including micro- and nanoelectronics, optoelectronics, biotechnology, and robotics. In Nature, many small animals exhibit reversible *dry* adhesion,[1–5] which has led to much research effort to mimic the structure and function of biological adhesives.[6–16] Generally, adhesion between two surfaces is strongly dependent on surface roughness and surface chemistry.[17] Lizards can cling on to and detach from many surfaces without regard to specific surface chemistry because of aligned fibrils on their feet.[1,18] It is well-known that adhesion between two elastomeric sheets can be controlled by temperature and tearing rate.[19] Meitl *et al.* recently have demonstrated transfer printing a wide range of objects onto a *smooth* substrate by kinetic control of adhesion of a PDMS stamp.[20] Here, we explore a new mechanism for regulating adhesion by adjusting the surface roughness on a wrinkled PDMS film simply by varying the stretch applied on the wrinkled film. It potentially offers a wider range of tunability and robustness than other approaches to "pick, transfer, and release" individual components with different sizes and shapes in real-time.

The PDMS strip with a rippled surface was fabricated following a procedure described earlier.[21] First, the PDMS strip was clamped (Fig. 1a) and mechanically stretched to an initial strain (ε_0) of 22.4% (Fig. 1b) in one direction. It was then subjected to oxygen plasma treatment in the stretched state (Fig. 1c) to generate a stiff and thin oxidized silicaceous layer on its top surface.[21] By partially releasing the initial strain (ε_0) to a critical level, an ordered periodic one-dimensional ripple pattern was formed spontaneously (Fig. 1d). Releasing the initial strain beyond the critical level increases the amplitude of these ripples (Fig. 1f–1h). If the sample is stretched back to ε_0, the surface returns to a flat state (Fig. 1e and 1i). Formation of a highly structured, rippled surface has been demonstrated by various groups through metal deposition[22,23] or surface oxidization[21,24,25] on an elastomer to generate a bi-layer structure, and by thermal expansion,[24] solvent swelling,[25] or mechanical stretching[21] to induce rippling. However, to our knowledge, there has been no attempt to control the adhesion in real-time *via* adjustment of the rippled surface by mechanical strain (Fig. 1d–1e), nor the quantitative understanding of changes in the adhesion in response to the strain.

Results and discussion

Our measure of adhesion comes from experiments in which a glass sphere indented the sample surface to a depth, Δ, of 10 μm, and was then retracted (Fig. 2a). The PDMS strip was mounted on an inverted optical microscope stage for indentation to measure the adhesive force at different strain levels (Fig. 3b). The motion of the stage was controlled by a motorized linear stage (see 'Materials and methods' for details). The sphere was retracted and the maximum force supported by the indenter (positive numbers represent tension), the pull-off force, F_{ad}, was our measure of adhesion. Fig. 3a shows force-displacement data from a series of experiments on a single sample at different values of strain (ε). Our measure of strain is defined as the following: if l_0 is the initial undeformed length of the PDMS substrate, ε is the released strain relative to the initial stretched state so that the deformed length of the specimen, $l = l_0(1 + \varepsilon_0 - \varepsilon)$. As shown in Fig. 3a, adhesion reduces systematically and significantly with the increase of ε, which is accompanied by an increase of ripple amplitude. These results suggest that strain offers an effective

[a]*Department of Materials Science and Engineering, University of Pennsylvania, 3231 Walnut Street, Philadelphia, PA, 19104, USA. E-mail: shuyang@seas.upenn.edu; Fax: +1 (215) 573-2128; Tel: +1 (215) 898-9645*
[b]*Department of Mechanical Engineering, National Taiwan University, No. 1, Sec. 4, Roosevelt Road, Taipei, 10617, Taiwan*
[c]*Department of Chemical Engineering, Lehigh University, 111 Research Drive, Bethlehem, PA, 18015, USA. E-mail: anj6@lehigh.edu; Fax: +1 (610) 758-5057; Tel: +1 (610) 758-4396*
[d]*Department of Theoretical and Applied Mechanics, Cornell University, 322 Thurston Hall, Ithaca, New York, 14853, USA*
† Electronic supplementary information (ESI) available: Optical images representing two different scenarios of the indentation process; full-length video of "pick and release" experiment. See DOI: 10.1039/b802848f

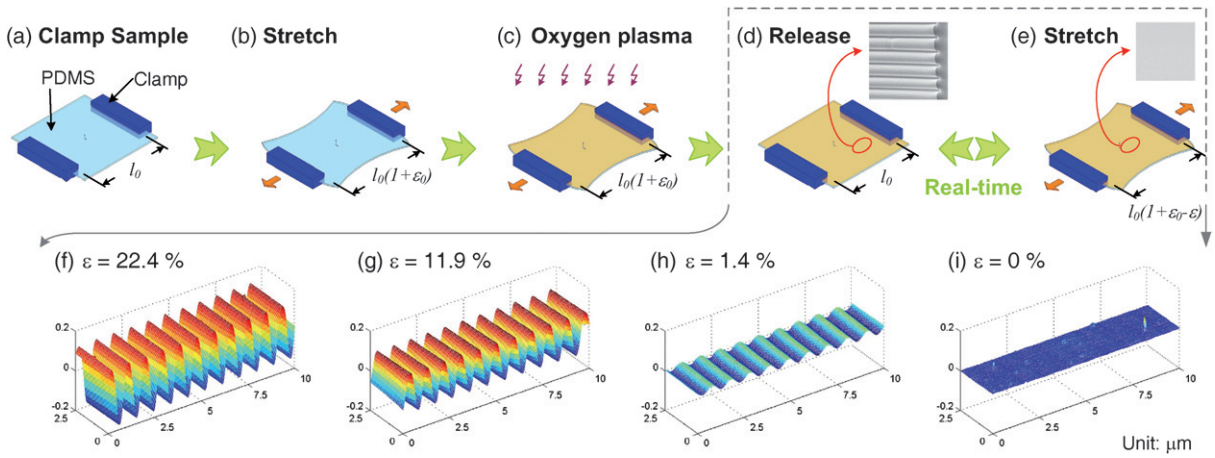

Fig. 1 Schematic illustration of the fabrication of rippled PDMS film (a–e) and real-time, reversible tunability of surface topography by mechanical strain (f–i). (a) Clamp PDMS film. (b) Stretch PDMS film to a designated strain value. (c) Oxygen plasma treatment. (d) Release stretch of the PDMS/oxide bilayer and spontaneous formation of ripple patterns. (e) Stretch back to the initial strain value and the ripple patterns disappear. (f–i) 3D surface contour of rippled surfaces measured by AFM and plotted using Matlab®.

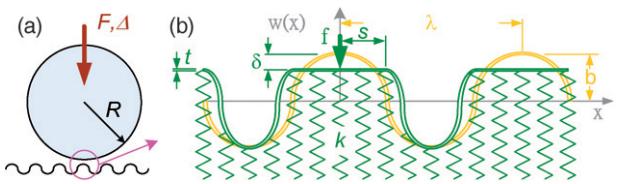

Fig. 2 (a) Illustrative sketch of the indentation process. (b) Blowup of (a) to illustrate modeling parameters and the deformed ripple geometry during indentation.

means for direct control of adhesion. Indeed, we can repeat the stretch–release cycle many times while maintaining these tunable adhesion characteristics. It is worth mentioning that our adhesion results are the opposite of a recent report by Crosby's group, where the wrinkled surface shows higher adhesion than the smooth film.[26] The latter was attributed to contact splitting mechanism, as suggested by gecko adhesion. We note that the wavelengths of our wrinkles (typically sub-micron to a few microns)[21] are two orders of magnitude smaller than those reported by Crosby's group.

To quantitatively understand how adhesion (pull-off force) varies as a function of strain, we have developed a contact mechanics model. Following the approach by Huck *et al.*,[27] the PDMS strip is modeled as an elastic foundation and the oxidized layer as a thin elastic plate (see Fig. 2b). During indentation at a fixed strain ε, the initial rippled surface can be either partially or completely flattened by the indenter. For both cases, we approximate the deformed shape of the plate, $w(x,\varepsilon)$, as

$$w(x,\varepsilon) = \begin{cases} -b' \cos\left(\dfrac{2\pi(x-\lambda/2)}{\lambda-2s}\right) - (\delta + b' - b) & |x| > s \\ b-\delta & |x| \le s \end{cases} \quad (1)$$

where λ, b are the wavelength and amplitude, respectively, of a ripple before indentation, and δ and $2s$ are the local deflection and contact width of each individual ripple, respectively. Eqn (1) assumes that the un-flattened part of the ripple retains

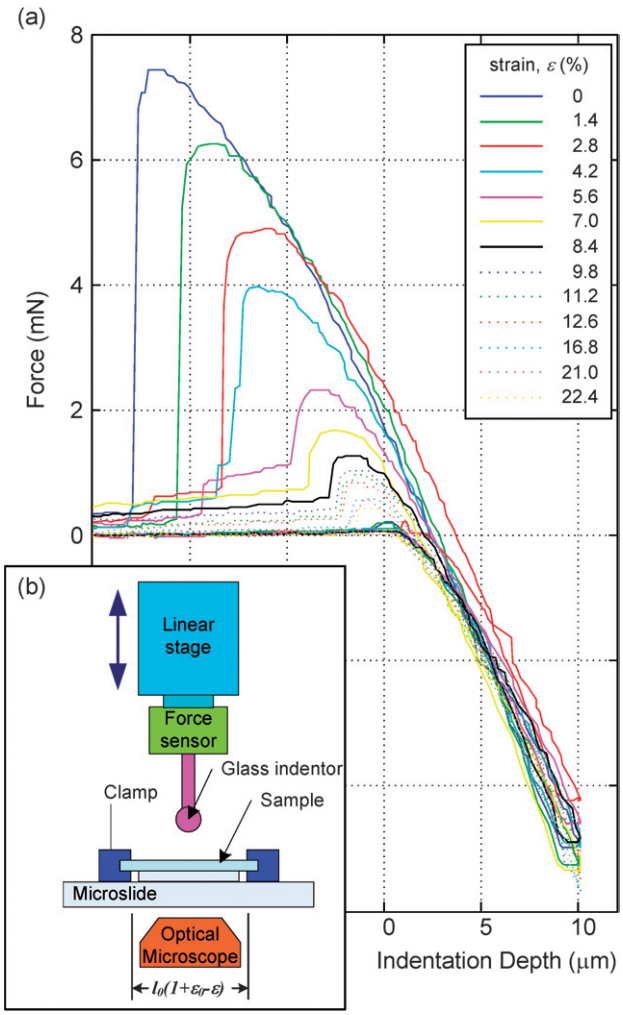

Fig. 3 Measurement of pull-off force on rippled PDMS films at different strain levels. (a) Plots of measured force and displacement during indentation of samples with different strains. (b) Setup of the indentation experiment.

a sinusoidal shape with amplitude b'. (Note that these quantities all depend on ε.) This approximation matches exactly the shape of the initial rippled surface prior to indentation, with $\delta,s = 0$ and $b' = b$.

The potential energy per unit projected area of the interface, U, is

$$U = U_b + U_c + U_s + U_{ad} \tag{2}$$

where U_b, U_c, U_s, U_{ad} are the bending energy, compression energy of the thin elastic plate, strain energy in the elastic foundation, and adhesion energy, respectively. They are calculated as

$$\begin{aligned} U_b &= \frac{\pi^4 b'^2 E_f^* t^3}{3\lambda(\lambda - 2s)^3} \\ U_c &= \tfrac{1}{2}E_f^* t\left(\frac{S_f}{S_i} - 1\right)^2 \\ U_s &= \frac{k}{\lambda}\left(\frac{\lambda}{2} - s\right)\left(\frac{b'^2}{2} + (\delta + b' - b)^2\right) + \frac{ks}{\lambda}(b - \delta)^2 \\ U_{ad} &= -2W_{ad}s/\lambda \end{aligned} \tag{3}$$

where E_f^* is the plane strain Young's modulus of the thin elastic plate, t is its thickness, I is moment of inertia, k is the spring constant of the foundation per unit length, ε is the mismatch strain, S_f and S_i are the final and initial (unstressed) lengths of the film, and W_{ad} is the work of adhesion between the glass indenter and the oxidized thin plate. The wavelength, λ, amplitude, b, and strain, ε, can be measured independently. W_{ad} can be estimated by the experimental results for very small roughness.

We first determine the predicted relationship between the initial ripple shape and strain ε. At a given strain, the initial ripple amplitude is defined as the amplitude that minimizes the total potential energy (U) with $b' = b$ and $\delta = s = 0$ in eqn (3). The amplitude determined using this procedure agreed well with our experiments. In addition, the ripple contour length depends only on ε_0 and is approximately independent of ε. This result was also well supported by our experiments (within ~6% error).

Our next step is to model the indentation process by considering two limiting cases:

Case I: low roughness or deep indentation, where the ripples are flattened everywhere in the contact except the area very near the contact edge (Fig. 4a and Fig. S1a†), and

Case II: high roughness or shallow indentation, where the ripples are slightly flattened and the contact area between all individual ripples and the indenter changes during indentation (Fig. 4c and Fig. S1b).

For case I, low roughness or deep indentation, the pull-off force F_{ad} is estimated using Johnson–Kendall–Roberts (JKR) theory,[28] that is,

$$F_{ad} = \frac{3}{2}W_{eff}\pi R \tag{4}$$

where R is the radius of the indenter and W_{eff} is the effective work of adhesion. It should be noted that in JKR theory the contacting surfaces are assumed to be smooth and the contact to be circular. We have observed experimentally that the contact remains approximately circular despite the anisotropy introduced in the surface by the ripples. On retraction of the indenter, energy is released from the bulk. In our case, additional energy is recovered by the system because the surface is rippled. Specifically, energy is released by the material elements ahead of the retracting contact edge as they recover from their flattened to rippled state. Following Persson and Tosatti,[29] we assume that this energy can be absorbed into the work of adhesion so that an effective work of adhesion can be defined as

where
$$W_{eff} = W_{ad} - U_r \tag{5a}$$

$$U_r = U_c|_{b'=b=s=\delta=0} - (U_b + U_s)|_{b'=b=b_{min};s=\delta=0} \tag{5b}$$

is the elastic energy per unit area released by the ripples when the contact decreases in size. Eqn (4) neglects the instabilities predicted on detachment of an adhesive rippled surface under plane strain conditions.[30–32] This assumption is supported by our experimental observation that when the contact radius was reduced, the contact edge retracted smoothly, avoiding the instabilities predicted in a 2D plane strain analysis. Under small amplitude approximation, it can be shown that the elastic energy released by ripples scales with amplitude as

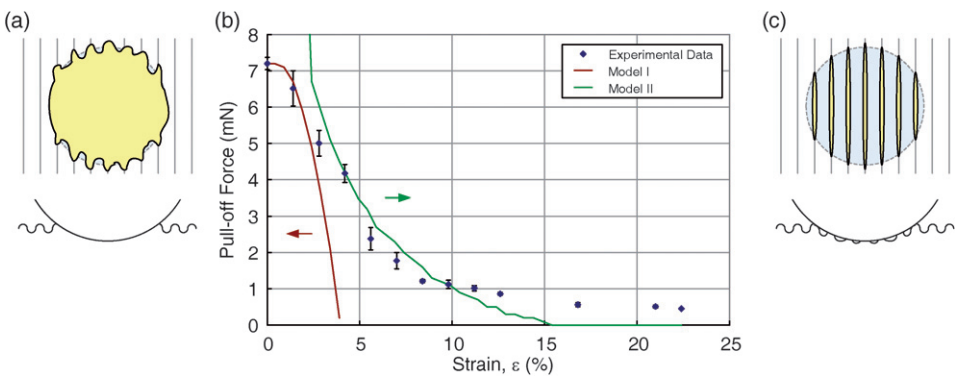

Fig. 4 (b) Comparison of experimental pull-off force *versus* strain to theoretical predictions from two limiting cases of contact mechanics models. (a) Model I for low roughness and deep indentation; ripples flatten everywhere in the contact except very near the contact edge. (c) Model II for high roughness and shallow indentation; ripples are partially flattened.

$$U_r = c_1 b^4 - c_2 b^2 \quad (6)$$

where c_1 and c_2 are constants. This strong reduction of adhesion with ripple amplitude implies that complete flattening of ripples is extremely expensive energetically as amplitude increases. It is far more likely that contact between the indenter and the rippled surface will be partial, as shown in Fig. 4c and Fig. S1b. Using eqn (4), we determined $W_{ad} = 381$ mN m^{-1} by conducting a pull-off force measurement with a flat smooth sample (fully-stretched, $\varepsilon = 0$). The relation of strain (ε) *versus* pull-off force (F_{ad}) is determined by eqn (5a) together with eqn (4).

When contact between the indenter and rippled surface is partial, a new model is considered (case II: high roughness or shallow indentation). The relation between strain and pull-off force is more complicated since energy exchange takes place over the entire contact area and not just at its edge. Thus, for a fixed strain ε, the model needs to compute the force-displacement response at each ripple locally. First, the shape of a partially flattened ripple (*i.e.*, b' and s) is established by minimizing the potential energy with respect to b' and s, for a fixed normal deflection, δ. Knowing the deformed shape of the ripple and using the contact condition allows us to determine the local force per unit area, f, on a ripple as a function of δ. This procedure is repeated for different values of δ to obtain the force–deflection response of an individual ripple. Fig. 5a shows a typical calculated force–deflection plot for $\varepsilon = 0.05$. This represents the constitutive behavior of each ripple. The total indenter force (F) at a given indenter displacement (Δ), is found by integrating f(δ) over the contact area (see Fig. 5b):

$$F = \int_0^{r_{max}} f(\delta(r)) 2\pi r \, dr \quad (7)$$

where the limits of integration are from the center of the contact to the radius at which f is at maximum tension. The pull-off force is the maximum in the indenter force–displacement (F–Δ) plot. The procedure is repeated for different values of strain, ε.

Fig. 4b shows a comparison of measured strain *versus* pull-off force and those predicted by the two models presented above. By fitting the simulated results with the experimental data, the plate thickness, t, and the elastic modulus of substrate, E_s*, are found to be 22 nm and 28 MPa, respectively (see details in the Experimental section). Except for these two parameters, all others in our models have been determined independently from experiments. The small-roughness model is accurate for only a very narrow range of strain (<4%) since the energy penalty to completely flatten ripples grows very rapidly with increasing amplitude. The partial-contact model is not expected to be accurate for small strains but is quantitatively accurate for intermediate strain (~4–13%). In addition, our model predicts stronger decay of pull-off force at large strains than the experiments. This we interpret as being due to energy losses associated with large deformation in these ripples that is not captured in our models, where the materials are treated as perfectly elastic. Nevertheless, our simple models capture the effect of strain on adhesion. Further discussion of their limitations and specific parameters used in the models can be found in the Experimental section. To illustrate the feasibility of real-time tunability of the new adhesive, we have performed a "pick and release" experiment using the rippled PDMS film. Fig. 6 shows a series of movie frames from this demonstration and the full movie is available in the ESI†. When the rippled PDMS film is fully stretched, the pull-off force is estimated as 2.14 mN using eqn (4) and $W_{ad} =$ 381 mN m^{-1}, exceeding the weight of a 3/32″-diameter glass ball, 1.33 mN. Thus, the adhesion force is sufficient to lift the ball as shown in Fig 6a–c. Upon strain release, when the roughness of PDMS strip is increased to a critical value, the glass ball drops due to loss of adhesion (Fig. 6d). The fact that the glass ball cannot be picked up in this configuration of PDMS further proves the loss of adhesion (Fig. 6e–g). The "pick and release" process can be controlled reversibly and repeatably.

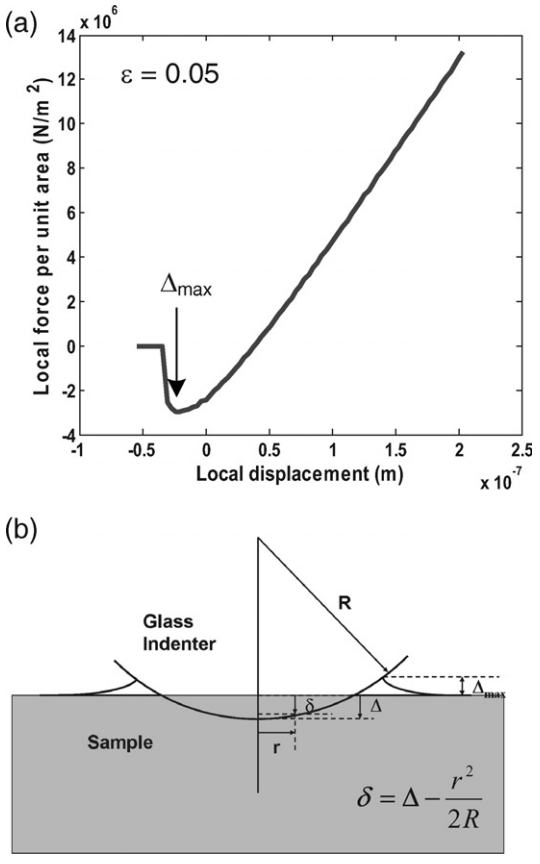

Fig. 5 (a) A typical force–deflection plot calculated according to the formulation in case II (ripples are partially flattened as shown in Fig. 4c). (b) Illustrative sketch of the indentation process to illustrate modeling parameters and their relations.

Conclusion

We believe that the demonstrated mechanical-strain-controlled dry adhesion mechanism based on regulating surface roughness may be valuable for the advancement of many existing technologies, including micro- and nanoelectronics and optoelectronics, as well as for driving new paradigms in biotechnology and soft robotics. The simplicity of the fabrication process and the wide range of possibility to manipulate different objects (size, shape and mass) using a single adhesive strip will be of considerable interest in production and materials handling that involves transferring, filtering, sorting and engagement/disengagement. The model presented here shows how adhesion to a periodically

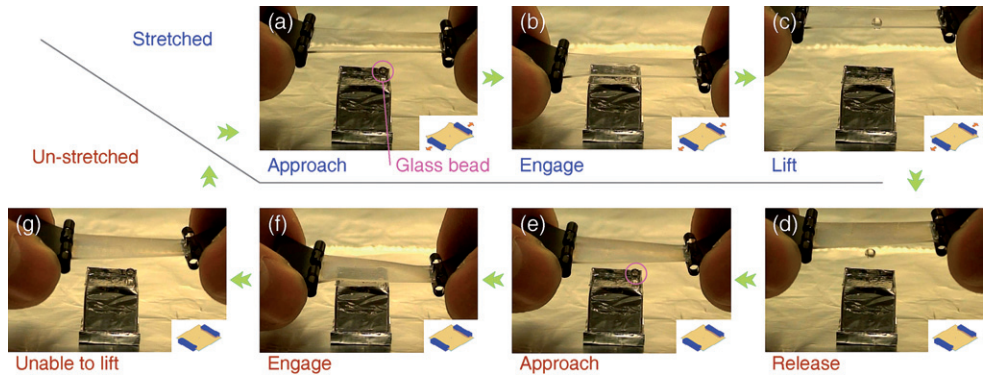

Fig. 6 Images of picking and release of a small glass sphere using the rippled PDMS film, demonstrating real-time tunable dry adhesion. A glass ball can be lifted up (a–c) when the rippled PDMS film is stretched flat (high adhesion), and dropped (d) as the stretch is released (reduced adhesion). When the sample is unstretched (rippled surface, low adhesion), the adhesion force is too low to lift the glass ball (e–g). Insets: Schematic drawings of the status of strain on the PDMS film. The full movie is available as ESI†.

rippled surface in the limit of small amplitude can be analyzed by extending JKR theory to account for energy released during rippling. For large amplitude ripples, we have presented a model that accounts for partial contact and that can be the basis for handling more complex structures. In addition, this methodology will offer valuable insights for the design of tunable friction and wetting behaviors based on surface topography. Besides the surface characteristics, the mechanochromatic color change in tunable periodic structures may find uses in light detection, lasing, sensing, and camouflage.

Experimental

PDMS sheet preparation

PDMS precursor (RTV615 from GE Silicones) was mixed with curing agent (10 : 1) and sandwiched between two 12″ × 3″ borosilicate flat-plate glasses using 0.5 mm-height shims as spacers. They were held together by 10 large 2″ binder clips and cured at 65 °C for 4 hours in a forced-air convection oven. After curing, the PDMS sheet (thickness of 0.5 ± 0.02 mm) was cut into 40 mm × 15 mm strips for experiment.

Ripple pattern generation[21]

The PDMS strip was clamped by two 3/4″ small binder clips with nominal length (l_0) of 25 mm and mounted on the custom-made stretching jig composed of one large acrylic base and two sliders, whose positions could be adjusted continuously in real-time by two 30 mm-long M4 wing screws with pitch 0.7 mm. The PDMS strip was then stretched to the designated initial strain level (ε_0, 22.4%, 8 turns of M4 wing screw), followed by exposure to oxygen plasma (Technics, model PE11-A) with power setting at 100 watts, time duration of 60 second, and pressure at 550 mTorr. Wrinkle patterns were formed spontaneously upon release of the strain, reaching the final shape when the external force was completely removed.

Sample characterization

Scanning electron microscopy (SEM) images were taken by FEI Strata DB235 Focused Ion Beam in high vacuum mode with acceleration voltage of 5 kV. Surface topography was imaged by a DI Dimension 3000 Atomic Force Microscope (AFM) in tapping mode, and the raw image data were imported into Matlab® to better illustrate the 3D surface. The adhesion force measurement setup is custom designed, consisting of inverted microscope (Olympus PMG3), miniature linear stage (Newport MFA-CC), load cell (transducer techniques, GSO-10), and an 8 mm-diameter glass indenter. In the indentation tests, the sample with controlled strain (ε) was fixed on top of the microscope stage, while the glass indenter was moved up and down at a speed of 1 μm s^{-1} and depth of 10 μm for each indentation cycle. The motion was controlled by a linear motorized stage and the force was collected through load cell located between the indenter and the motor. Force data and linear stage position were collected by NI LabView 8.0 program. Demonstration of "pick and release" was captured on video by a SONY HDR-HC1 HD video camera and edited by Mac iMovie.

Further details on the model and parameter estimation

The spring constant (k) was determined by equating the normal interfacial stress to that obtained from the exact half space solution.[27,33] It is related to the elastic modulus of the substrate and wavelength as shown in the following equation:

$$k = \frac{4\pi E_s^*}{(3-\nu_s^*)(1+\nu_s^*)\lambda} \tag{7}$$

where λ, b and ε can be measured independently. As mentioned in the paper, the work of adhesion (W_{ad}) was calculated using eqn (4) and the measured pull-off force of a fully stretched ($\varepsilon = 0$) sample. In the models, λ was assumed to be independent of the strain and was taken to be the critical buckling wavelength, which depends only on the plate thickness (t) and the ratio of elastic moduli of the plate and the PDMS strip, E_f^*/E_s^*.[27,33] Therefore, knowing λ allows us to determine E_f^* by solving for E_s^* and t. To determine E_s^* and t, we fitted the theoretical pull-off force as a function of strain to the experimental data in the partial contact regime, which gave $E_s^* = 28$ MPa and $t = 22$ nm. As pointed by Huck *et al.*,[27] oxidation can substantially increase the elastic modulus of a sub-surface layer of the PDMS substrate,

resulting in a much higher effective modulus of the substrate. We confirmed this by performing an indentation test on an oxidized flat PDMS substrate, and found that E_s* was equal to 8.9 MPa, which was much higher than the bulk value of 2.6 MPa, although still considerably lower than that was required to fit our data. Note that the indentation test probes much greater depths than those strained under shallow indentation, a few microns. An upper limit for plate thickness ($t = 25$ nm) can be established by noting that ripples cannot form below a certain critical strain, and a lower limit of $t = 7$ nm can be estimated from the known stiffness of pure silica.[34] The plate thickness needed to fit our data falls within these limits. The models we have presented here are based on several simplified assumptions. The potential energy is evaluated based on an initial state where a stress-free PDMS strip is stretched to a strain ε, followed by removal of the strain completely, leading to the formation of ripples. This is different from the experimental situation, where the residual strain exists in the system after unloading as $\varepsilon_0 - \varepsilon$. Only within the spring foundation model is there no difference between the two situations. Since our foundation stiffness is chosen so that the normal stress on the interface between the oxidized film and the PDMS strip matches the exact solution of the rippling problem,[27,33] it implies that we have neglected the additional compliance due to the foundation. This also means that our analysis of the large-amplitude ripples will break down for large indentation or low ripples. Finally, in current version of the model there are always many internal interfaces. Therefore, the pull-off force increases without bound as strain decreases. In reality there will be a transition to a contact with no internal interfaces, which is captured by the first model.

Optical images demonstrating the two different contact scenarios, fully flattened *vs.* partially flattened, can be found in the ESI†.

Acknowledgements

We gratefully thank Daniel E. Koditschek for helpful discussions and John Bassani for critical reading of the manuscript. This work has been partially supported by National Science Foundation (NSF) awards # DMR-0548070 and CMS-0527785. S.Y. also acknowledges the 3 M Non-tenured Faculty Grant.

References

1 K. Autumn, Y. A. Liang, S. T. Hsieh, W. Zesch, W. P. Chan, T. W. Kenny, R. Fearing and R. J. Full, *Nature*, 2000, **405**, 681–685.
2 T. Eisner and D. J. Aneshansley, *Proc. Natl. Acad. Sci. U. S. A.*, 2000, **97**, 6568–6573.
3 S. N. Gorb, *Proc. R. Soc. London, Ser. B*, 1998, **265**, 747–752.
4 G. Huber, H. Mantz, R. Spolenak, K. Mecke, K. Jacobs, S. N. Gorb and E. Arzt, *Proc. Natl. Acad. Sci. U. S. A.*, 2005, **102**, 16293–16296.
5 K. Autumn, M. Sitti, Y. C. A. Liang, A. M. Peattie, W. R. Hansen, S. Sponberg, T. W. Kenny, R. Fearing, J. N. Israelachvili and R. J. Full, *Proc. Natl. Acad. Sci. U. S. A.*, 2002, **99**, 12252–12256.
6 A. K. Geim, S. V. Dubonos, I. V. Grigorieva, K. S. Novoselov, A. A. Zhukov and S. Y. Shapoval, *Nat. Mater.*, 2003, **2**, 461–463.
7 J. Y. Chung and M. K. Chaudhury, *J. R. Soc., Interface*, 2005, **2**, 55–61.
8 A. Ghatak, L. Mahadevan, J. Y. Chung, M. K. Chaudhury and V. Shenoy, *Proc. R. Soc. London, Ser. A*, 2004, **460**, 2725–2735.
9 N. J. Glassmaker, A. Jagota, C. Y. Hui and J. Kim, *J.R. Soc. Interface*, 2004, **1**, 23–33.
10 C. Y. Hui, N. J. Glassmaker, T. Tang and A. Jagota, *J.R. Soc. Interface*, 2004, **1**, 35–48.
11 N. J. Glassmaker, A. Jagota, C. Y. Hui, W. L. Noderer and M. K. Chaudhury, *Proc. Natl. Acad. Sci. U. S. A.*, 2007, **104**, 10786–10791.
12 S. Kim and M. Sitti, *Appl. Phys. Lett.*, 2006, **89**, 3.
13 C. Greiner, A. del Campo and E. Arzt, *Langmuir*, 2007, **23**, 3495–3502.
14 L. Ge, S. Sethi, L. Ci, P. M. Ajayan and A. Dhinojwala, *Proc. Natl. Acad. Sci. U. S. A.*, 2007, **104**, 10792–10795.
15 Y. Tian, N. Pesika, H. B. Zeng, K. Rosenberg, B. X. Zhao, P. McGuiggan, K. Autumn and J. Israelachvili, *Proc. Natl. Acad. Sci. U. S. A.*, 2006, **103**, 19320–19325.
16 N. S. Pesika, Y. Tian, B. X. Zhao, K. Rosenberg, H. B. Zeng, P. McGuiggan, K. Autumn and J. N. Israelachvili, *J. Adhes.*, 2007, **83**, 383–401.
17 S. Minko, M. Muller, M. Motornov, M. Nitschke, K. Grundke and M. Stamm, *J. Am. Chem. Soc.*, 2003, **125**, 3896–3900.
18 K. Autumn, A. Dittmore, D. Santos, M. Spenko and M. Cutkosky, *J. Exp. Biol.*, 2006, **209**, 3569–3579.
19 A. N. Gent, *Langmuir*, 1996, **12**, 4492–4496.
20 M. A. Meitl, Z. T. Zhu, V. Kumar, K. J. Lee, X. Feng, Y. Y. Huang, I. Adesida, R. G. Nuzzo and J. A. Rogers, *Nat. Mater.*, 2006, **5**, 33–38.
21 P. Lin and S. Yang, *Appl. Phys. Lett.*, 2007, **90**, 241903.
22 N. Bowden, S. Brittain, A. G. Evans, J. W. Hutchinson and G. M. Whitesides, *Nature*, 1998, **393**, 146–149.
23 P. J. Yoo, K. Y. Suh, S. Y. Park and H. H. Lee, *Adv. Mater.*, 2002, **14**, 1383–1387.
24 N. Bowden, W. T. S. Huck, K. E. Paul and G. M. Whitesides, *Appl. Phys. Lett.*, 1999, **75**, 2557–2559.
25 E. P. Chan and A. J. Crosby, *Soft Matter*, 2006, **2**, 324–328.
26 E. P. Chan, E. J. Smith, R. C. Hayward and A. J. Crosby, *Adv. Mater.*, 2008, **20**, 711–716.
27 W. T. S. Huck, N. Bowden, P. Onck, T. Pardoen, J. W. Hutchinson and G. M. Whitesides, *Langmuir*, 2000, **16**, 3497–3501.
28 K. L. Johnson, *Contact Mechanics*, Cambridge University Press, 1985.
29 B. N. J. Persson and E. Tosatti, *J. Chem. Phys.*, 2001, **115**, 5597–5610.
30 K. L. Johnson, *Int. J. Solids Struct.*, 1995, **32**, 423–430.
31 C. Y. Hui, Y. Y. Lin, J. M. Baney and E. J. Kramer, *J. Polym. Sci., Part B: Polym. Phys.*, 2001, **39**, 1195–1214.
32 P. R. Guduru, *J. Mech. Phys. Solids*, 2007, **55**, 445–472.
33 H. G. Allen, *Analysis and Design of Structural Sandwich Panels*, 1st edn, Pergamon Press, London, 1969.
34 W. D. Kingery, H. K. Bowen and D. R. Uhlmann, *Introduction to Ceramics*, 2nd edn, Wiley-Interscience, New York, 1976.